Supporting Information

Unveiling the Chemical Reconstruction of $Fe(OH)_3$-Embedded Ni-MOF Nanorods for Enhanced Oxygen Evolution Reaction

Da Ye,[+] Luhong Fu,[+] Yan Tang,[+] Ding Zhang, Teng Liu*

Corresponding Author

Teng Liu — School of Chemical Engineering and Pharmacy

Wuhan Institute of Technology Wuhan, Hubei 430205, P. R. China

Email: tliu@wit.edu.cn

1. Materials and Methods

Materials

$Ni(NO_3)_2{\cdot}6H_2O$, $FeCl_3$, NH_4F, urea and imidazole are all analytical pure from Shanghai Aladdin Biochemical Technology, China. Nickel foam (NF) was purchased from Suzhou Ke Sheng Metal Materials company, China. Nafion solution (5% in isopropanol) was supplied by Sigma-Aldrich, Germany.

Synthesis of $Ni(OH)_2$

The nickel foam (NF) was ultrasonically cleaned in acetone, ethanol, 3 M HCl and ultrapure (UP) water for 10 minutes each. A solution was prepared by dissolving 1 mmol $Ni(NO_3)_2{\cdot}6H_2O$, 4 mmol NH_4F, and 5 mmol $CO(NH_2)_2$ in 15 mL UP water and transferred to a 22 mL Teflon-sealed autoclave. A piece of cleaned NF was diagonally placed in the solution, then it was heated to 120 °C at a rate of 5 °C / min and maintained for 8 h. After natural cooling, the NF was rinsed three times with UP water, yielding $Ni(OH)_2$ grown on the NF.

Synthesis of Ni-MOF

A circular quartz tube (2.5 cm in diameter, 10 cm in length) was used as the reaction vessel. Imidazole powder (10 mmol) was placed at the sealed end, with a piece of nickel foam (NF) coated with $Ni(OH)_2$ positioned at the tube's midpoint. The system was then heated to 280 °C at a rate of 5 °C/min under a nitrogen atmosphere in a tube furnace and held at this temperature for 1 hour. After natural cooling, the Ni-MOF grown on NF was carefully retrieved from the quartz tube.

Synthesis of Fe/Ni-MOF

The Ni-MOF was etched using a 0.15 M $FeCl_3$ solution for 15 minutes at room temperature. The resulting product was then thoroughly washed with UP water until the filtrate turned colorless, followed by drying in a vacuum oven to obtain Fe/Ni-MOF grown on NF. Control samples were prepared by etching Ni-MOF in $FeCl_3$ solutions of varying concentrations (0.01, 0.05, 0.1, 0.2, and 0.25 M) for 15 minutes, or by treating with 0.15 M $FeCl_3$ solution for 5, 10, 20, and 25 minutes to determine the optimal etching conditions.

Synthesis of $Fe/Ni(OH)_2$

$Fe/Ni(OH)_2$ grown on NF was prepared following a similar protocol to that used for

Fe/Ni-MOF, with the primary difference being the substitution of Ni-MOF with $Ni(OH)_2$.

Electrochemical Measurements

Potential Calibration

All electrochemical measurements were conducted on a CHI-760E electrochemical workstation with a conventional three-electrode configuration in 1 M KOH. Potentials were calibrated to the reversible hydrogen electrode (RHE) using the equation:

$$E_{RHE} = E_{measured} - \Delta V - 50\% iR$$

The zero intercept (ΔV, –0.919 V) was determined through the cyclic voltammetry (CV) of the hydrogen electrode reaction of Pt in 1 M KOH saturated with H_2. The electrolyte resistance (R) was approximately 1.7 Ω, and all the potential has been calibrated to RHE (E_{RHE}).

Electrode Preparation

A Hg/HgO electrode (filled with 1 M KOH) and a carbon rod (5 mm diameter, 8 cm length) were served as the reference and counter electrode, respectively. $Ni(OH)_2$, Ni-MOF, Fe/$Ni(OH)_2$, and Fe/Ni-MOF samples (1 cm × 1 cm) were directly affixed to the working electrode for electrochemical tests. Specifically, the working electrode is clamped with an electrode clamp, and the exposed portion (0.6 cm × 1 cm) of the electrode is just immersed into the solution. For IrO_2, a conventional electrocatalyst ink was prepared and deposited onto a rotating disk electrode (RDE) with a loading of 0.5 mg/cm^2, using several drops of 0.1% Nafion solution to secure the electrocatalyst on the electrode.

Electrochemical Test Methods

Prior to characterization, all electrocatalysts underwent an activation process, which involved continuous CV scanning from 1.22 V to 1.77 V at a rate of 0.5 V/s until the last two cycles converged. CV curves were recorded from 1.22 V to 1.77 V at a scanning rate of 2 mV/s, with the negative-sweep half-cycle taken as the LSV curves. Tafel plots were generated from the linear regions of the LSV curves at low overpotentials and fitted to the Tafel equation:

$$\eta = b \log j + a$$

where η is overpotential, j is current density, and b is the Tafel slope.

Electrochemical impedance spectroscopy (EIS) measurements were performed at the open circuit potential (OCP). The current density near OCP showed a linear dependence on scanning rates, with the slope used to estimate the double-layer capacitance (Cdl). CVs were conducted over the range OCP ± 50 mV with scanning rates of 20, 40, 60, 80, 100, 120, and 140 mV/s, measuring current density at OCP to determine C_{dl}. The electrochemically active surface areas (ECSA) of $Ni(OH)_2$, Ni-MOF, Fe/$Ni(OH)_2$, and Fe/Ni-MOF were calculated as:

$$ECSA = Cdl/Cs$$

where C_s is the specific capacitance, treated as a constant for similar materials. Continuous CV was conducted from 1.22 to 1.77 V at a scan rate of 50 mV/s.

Chronoamperometric tests on Fe/Ni-MOF were performed at current densities of 10, 100, and 200 mA/cm^2.

In-situ Raman and UV spectra were collected after 20 minutes of operation at the specified voltages.

2.First-Principal Calculation

Density functional theory (DFT) calculations were conducted using the CASTEP module within the Materials Studio program developed by Bio Accelrys. The exchange-correlation interactions were modeled using the generalized gradient approximation (GGA) with the Perdew-Burke-Ernzerh (PBE) functional.[1, 2] Ultrasoft pseudopotentials were employed to account for interactions between valence electrons and ionic cores. The crystal structure of NiFe layered double hydroxide (LDH) was adopted from the literature.[3]

A four-layer 2 × 2 supercell of (001) slabs, both with and without an adsorbed carbonate ion, was constructed to simulate NiFe LDH and CO_3-NiFe LDH, respectively. In this configuration, each of the carbonate ion's oxygen atoms bonds to a Ni and an Fe atom, while the Ni/Fe atomic ratio remains 1:1. For each model, a vacuum gap of 15 Å was applied, with the atoms in the bottom two layers fixed and all other atoms fully optimized. Electronic wave functions were expanded on a plane wave basis with a cut-off energy of 380 eV, while a 2 × 2 × 1 Monkhorst-Pack grid k-point sampling was used for geometric optimizations. The convergence thresholds were set to 1×10^{-6} eV in energy and 0.02 eV/Å in force. Additionally, van der Waals interactions were described using the DFT-D2 method by Grimme.[4]

The adsorption free energies for intermediates OH_ad, O_ad, and OOH_ad were calculated using the formula $\Delta G = \Delta E + \Delta ZPE - T\Delta S$, where ΔE, ΔZPE, and ΔS correspond to the binding energy, zero-point energy change, and entropy change of the adsorption process, respectively.[5, 6]

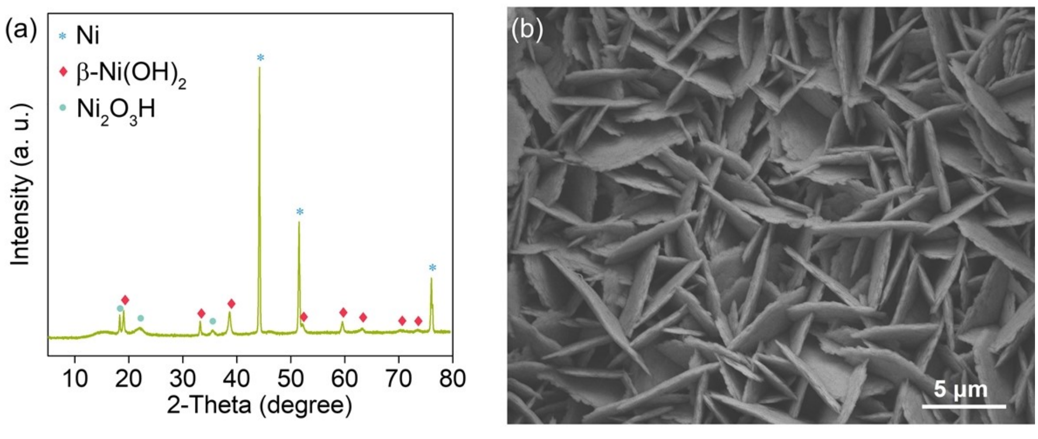

Figure S1 (a) XRD patterns and (b) SEM image of $Ni(OH)_2$.

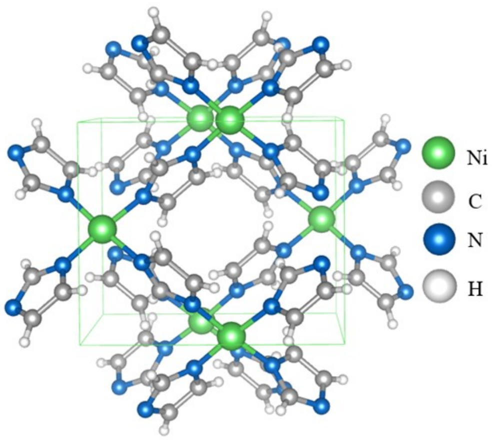

Figure S2 Unit cell atom model of Ni-MOF.

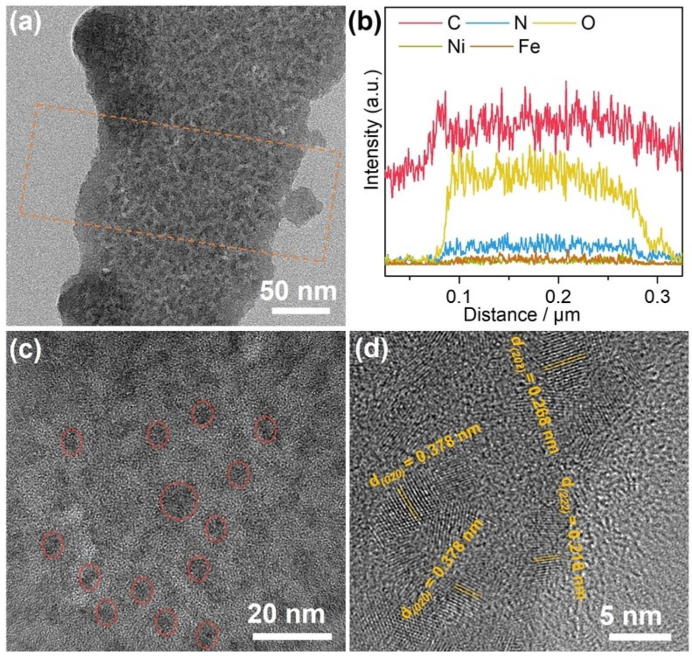

Figure S3 TEM image (a), line scanning (b), HRTEM image, HRTEM image with lattice spacing (d) of Fe/Ni-MOF. Red circle in (c): $Fe(OH)_3$ nanoparticles.

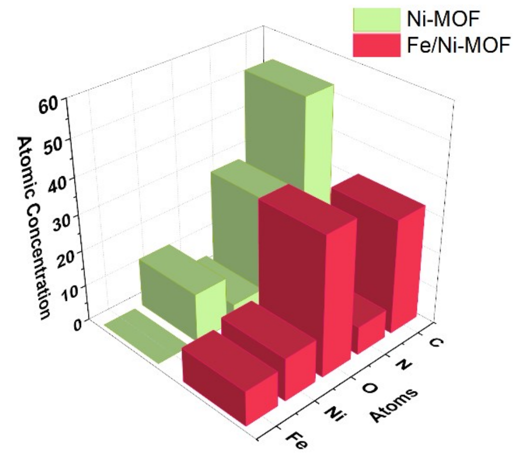

Figure S4 The atomic concentrations of C, N, O, Ni, and Fe in Fe/Ni-MOF compared with Ni-MOF.

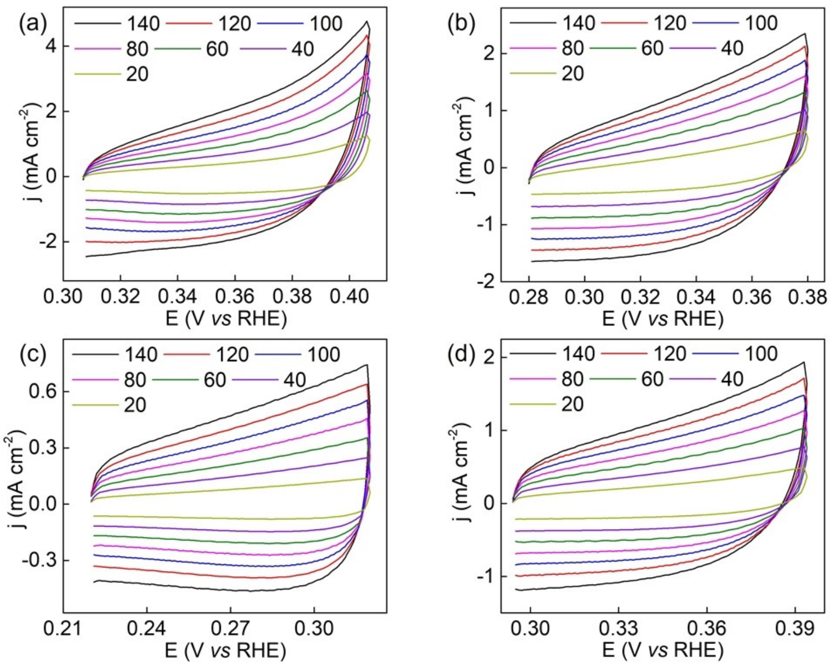

Figure S5 CV curves between OCP ± 50 mV for $Ni(OH)_2$ (a), Fe/$Ni(OH)_2$ (b), Ni-MOF(c) and Fe/Ni-MOF(d) at scan rates of 20, 40, 60, 80, 100, 120, 140 mV s^{-1}.

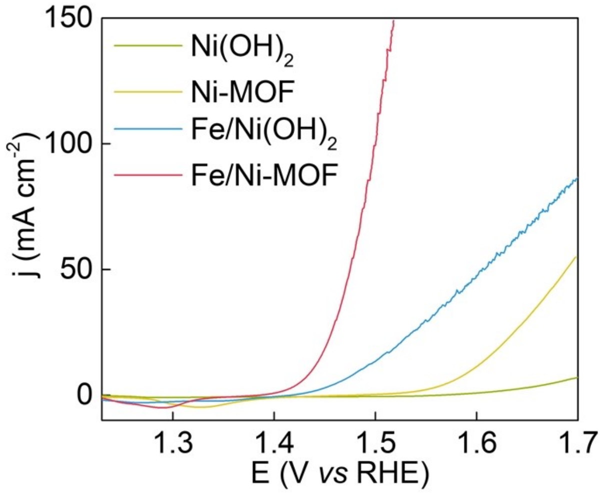

Figure S6 ECSA-normalized LSV curves of $Ni(OH)_2$ (a), $Fe/Ni(OH)_2$ (b), Ni-MOF(c) and Fe/Ni-MOF(d).

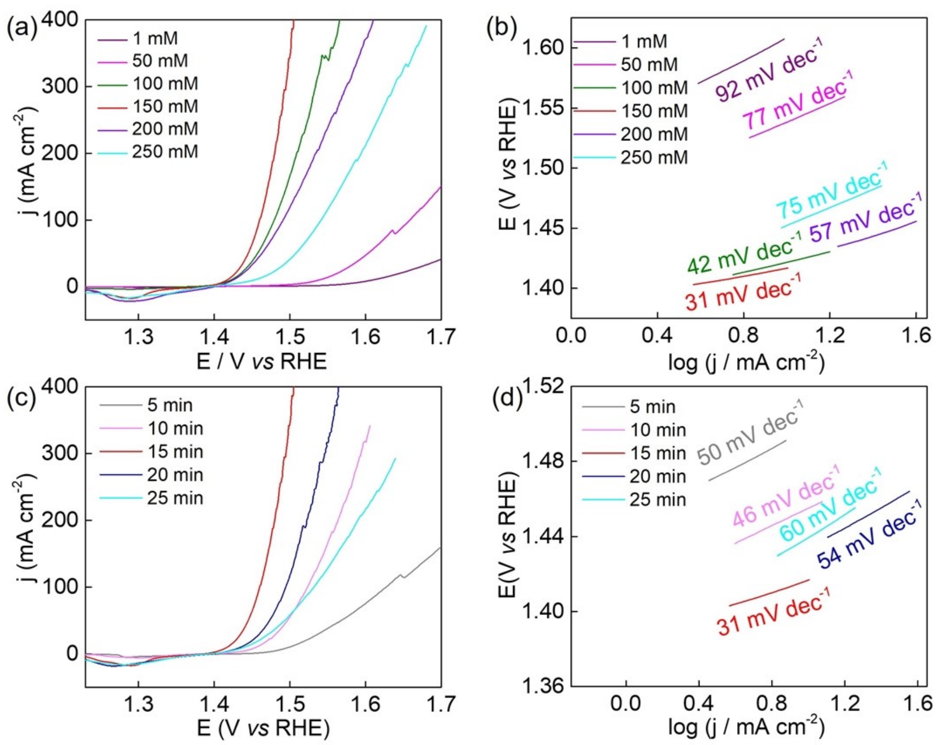

Figure S7 LSV curves (a) and Tafel plots (b) of Ni-MOF immersed in $FeCl_3$ solution with various concentrations (1 mM to 250 mM) for 15 minutes. LSV curves (c) and Tafel plots (d) of Ni-MOF immersed in 0.15 M $FeCl_3$ solution for durations ranging from 5 to 25 minutes.

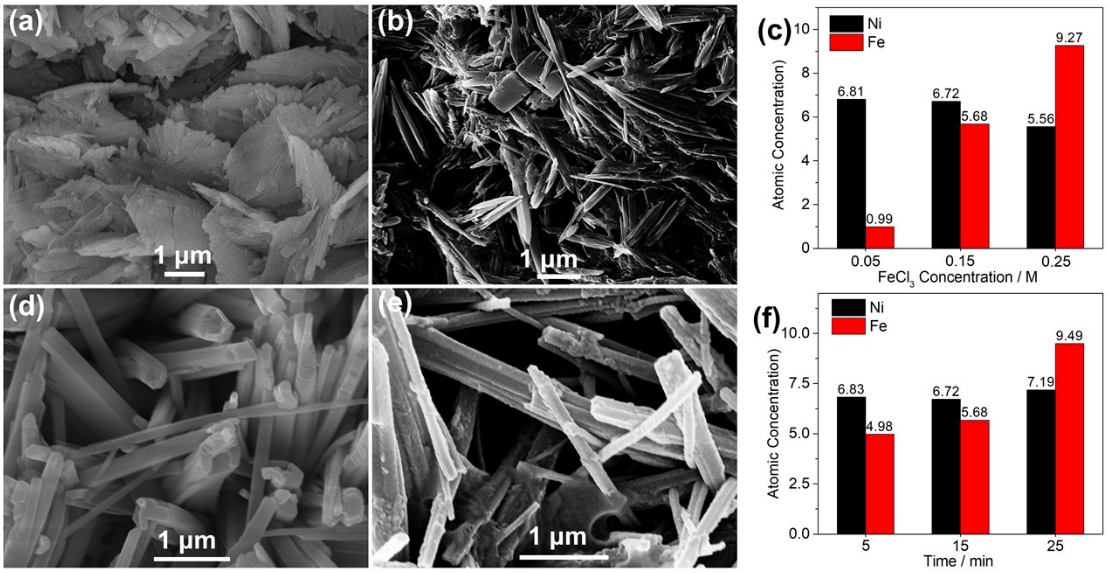

Figure S8 SEM images of Fe/Ni-MOF etching with 0.05 M (a) and 0.25 M (b) $FeCl_3$ for 15 min, and 0.15 M for 5 min (d) and 25 min (e). ICP-OER results of Fe/Ni-MOF etching with 0.05/0.15/0.25 M $FeCl_3$ for 15 min (c) and 0.15 M for 5/15/25 min (e).

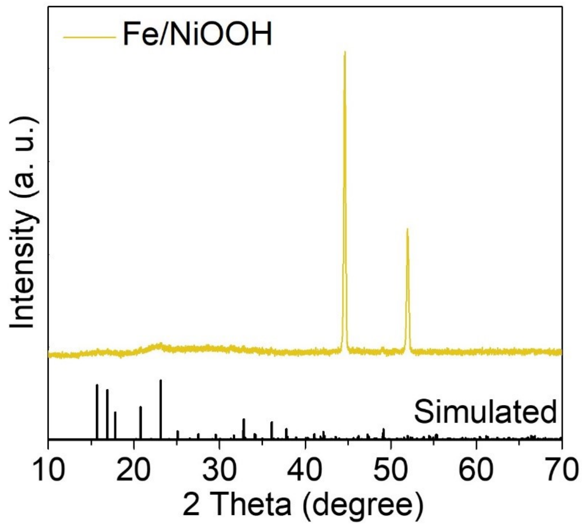

Figure S9 XRD pattern of Fe/NiOOH.

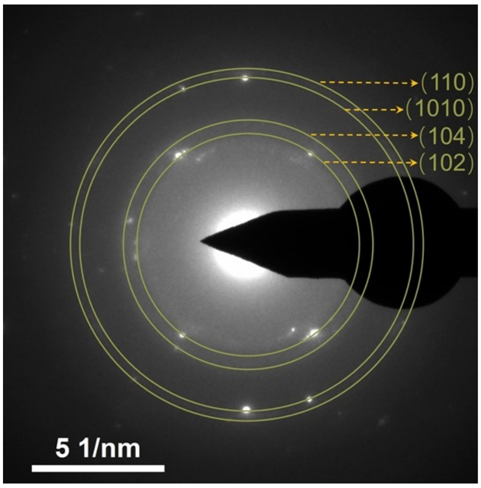

Figure S10 The selected area electron diffraction (SAED) pattern of Fe/NiOOH.

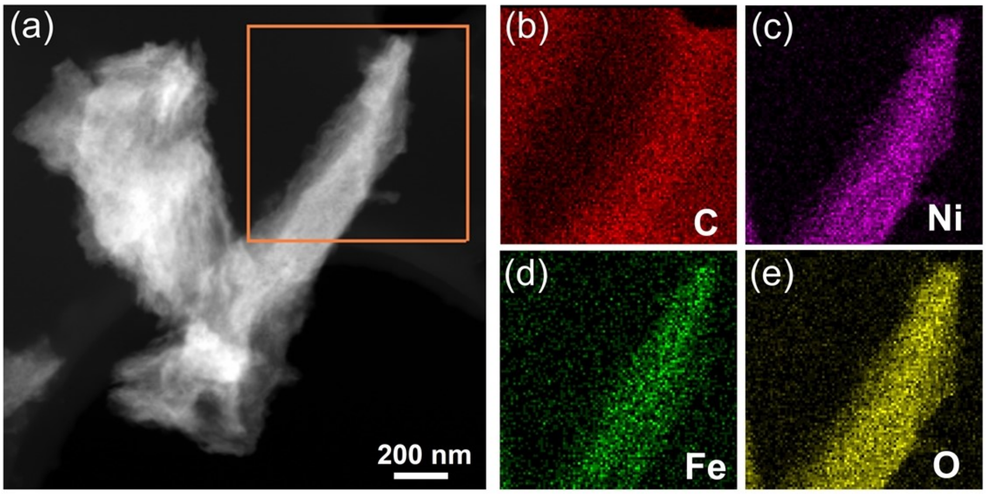

Figure S11 HAADF-STEM (a), EDS elemental mapping of C (b), Ni (c), Fe (d) and O (e) of Fe/NiOOH.

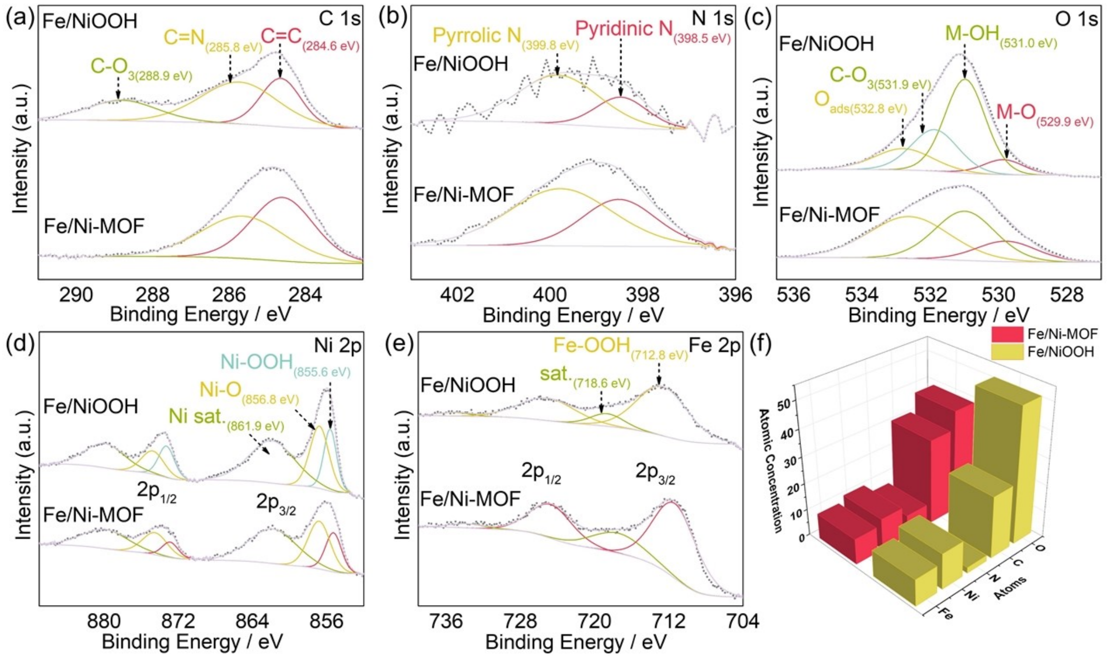

Figure S12 The high-resolution XPS spectra of C 1s (a), N 1s (b), O 1s (c), Ni 2p (d), Fe 2p (e) and the atomic concentrations of O, C, N, Ni and Fe (f) of Fe/Ni-MOF and Fe/NiOOH.

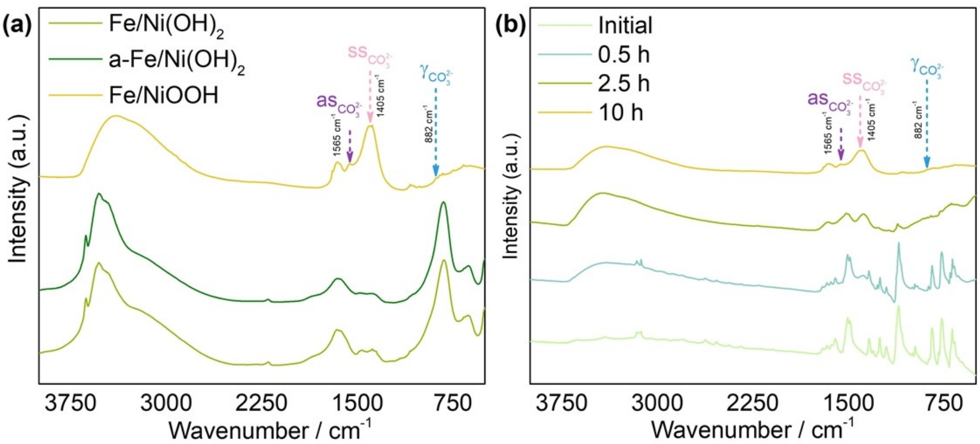

Figure S13 FT-IR spectroscopy of $Fe/Ni(OH)_2$, a-$Fe/Ni(OH)_2$ and Fe/NiOOH (a), and Fe/NiOOH with different durations at current density of 200 mA cm^{-2} (b).

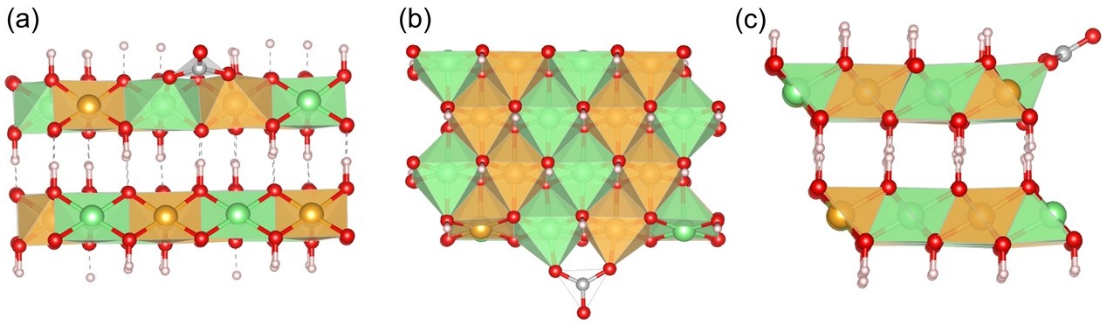

Figure S14 The front view (a), top view (b), and side view (c) of CO_3^{2-}-adsorbed Fe/NiOOH models.

Table S1 Atomic parameters of Ni-MOF.

Phase data	
Space-group	P b c n (60) - orthorhombic
Cell	a=7.388(3) Å b=8.755(4) Å c=10.489(4) Å a/b=0.8439 b/c=0.8347 c/a=1.4197 V=678.45(50) Å^3 Z=4

Atomic parameters						
Atom	Wyck.	Site	x/a	y/a	z/c	U [Å^2]
Ni1	4c	.2.	0	0.56710(3)	1/4	
N1	8d	1	0.1592(2)	0.41864(15)	0.31673(16)	
N2	8d	1	0.3531(2)	0.22466(15)	0.31590(15)	
C1	8d	1	0.2163(2)	0.20191(19)	0.2571(2)	
H1	8d	1	0.167(3)	0.258(2)	0.182(2)	0.0270
C2	8d	1	0.2686(3)	0.4305(2)	0.4221(2)	
H2	8d	1	0.254(4)	0.509(2)	0.482(2)	0.0330
C3	8d	1	0.3865(3)	0.3125(2)	0.42149(19)	
H3	8d	1	0.487(3)	0.288(2)	0.478(2)	0.0320

Table S2. Comparisons of OER performance for various electrocatalysts in 1.0 M KOH from other publications

Catalyst	Overpotential @10 mA cm^{-2} [mV]	Tafel slope [mV dec^{-1}]	
Fe/Ni-MOF	188	32	（this work）
Co-C/ZIF@CC (0.4 W)	290	59	[7]
(Ni,Fe)P(S,Se)$_3$	210	34	[8]

Co/Aza-CMP/CP	289	44	9
a-NiCo/NC	252	49	10
CoFe-N-C	360	68	11
W-$NiS_{0.5}Se_{0.5}$	171	41	12
$CoFeWO_x$	211	32	13
Ni/$NiFeMoO_x$	255	35	14
Ni-ZIF/Ni-B@nf	234	57	15
NiTe/NiS	209	49	16
$VCoCO_x$@NF	240	64	17
CuO@CoOOH/CF	186	51.7	18
$(Ni_2Co_1)_{0.925}Fe_{0.075}$-MOF	257	41.3	19

References

1. D. Vanderbilt, *Phys. Rev. B*, 1990, **41**, 7892-7895.
2. J. P. Perdew, K. Burke and M. Ernzerhof, *Phys. Rev. Lett.*, 1996, **77**, 3865.
3. Q. Hu, Y. F. Xue, J. X. Kang, I. Scivetti, G. Teobaldi, A. Selloni, L. Guo and L.-M. Liu, *ACS. Catal.*, 2021, **12**, 295-304.
4. S. Grimme, *J. Comput. Chem.*, 2006, **27**, 1787-1799.
5. P. Ferrin, A. U. Nilekar, J. Greeley, M. Mavrikakis and J. Rossmeisl, *Surf. Sci.*, 2008, **602**, 3424-3431.
6. J. K. Nørskov, T. Bligaard, A. Logadottir, J. Kitchin, J. G. Chen, S. Pandelov and U. Stimming, *J. Electrochem. Soc.*, 2005, **152**, J23.
7. W. H. Liu, J. Yang, Y. Z. Zhao, X. M. Liu, J. Heng, M. H. Hong, Y. W. Zhang and J. Wang, *Adv. Mater.*, 2023, **36**, 2310106.
8. W. W. Li, C. Li, H. L. Dong, X. L. Zhang, J. X. Liu, M. Song, G. Wang, L. Zhao, H. W. Sheng, B. Chen and H. Z. Zhang, *Angew. Chem. Int. Ed.*, 2023, **62**, e202214570.
9. H. Yang, F. S. Li, S. Q. Zhan, Y. W. Liu, W. L. Li, Q. J. Meng, A. Kravchenko, T. Q. Liu, Y. Yang, Y. Fang, L. Q. Wang, J. Q. Guan, I. Furó, M. S. G. Ahlquist and L. C. Sun, *Nat. Catal.*, 2022, **5**, 414-429.
10. Z. H. Pei, X. F. Lu, H. B. Zhang, Y. X. Li, D. Y. Luan and X. W. Lou, *Angew. Chem. Int. Ed.*, 2022, **61**, e202207537.
11. X. Y. Zhou, J. J. Gao, Y. X. Hu, Z. Y. Jin, K. L. Hu, K. M. Reddy, Q. H. Yuan, X. Lin and H.-J. Qiu, *Nano. Lett.*, 2022, **22**, 3392-3399.
12. Y. Wang, X. P. Li, M. M. Zhang, J. F. Zhang, Z. L. Chen, X. R. Zheng, Z. L. Tian, N. Q. Zhao, X. P. Han, K. Zaghib, Y. Wang, Y. D. Deng and W. B. Hu, *Adv. Mater.*, 2022, **34**, 2107053.
13. J. S. Chen, H. Li, Z. X. Yu, C. Liu, Z. W. Yuan, C. J. Wang, S. L. Zhao, G. Henkelman, S. Z. Li, L. Wei and Y. Chen, *Adv. Energy. Mater.*, 2020, **10**, 2002593.
14. Y. K. Li, G. Zhang, W. T. Lu and F. F. Cao, *Adv. Sci.*, 2020, **7**, 1902034.

15. H. B. Xu, B. Fei, G. H. Cai, Y. Ha, J. Liu, H. X. Jia, J. C. Zhang, M. Liu and R. B. Wu, *Adv. Energy. Mater.*, 2020, **10**, 1902714.
16. Z. Q. Xue, X. Li, Q. L. Liu, M. K. Cai, K. Liu, M. Liu, Z. F. Ke, X. L. Liu and G. Q. Li, *Adv. Mater.*, 2019, **31**, 1900430.
17. A. Meena, P. Thangavel, A. S. Nissimagoudar, A. N. Singh, A. Jana, D. S. Jeong, H. Im and K. S. Kim, *Chem. Eng. J.*, 2022, **430**, 132623.
18. J. Hu, A. Al‐Salihy, J. Wang, X. Li, Y. F. Fu, Z. H. Li, X. J. Han, B. Song and P. Xu, *Adv. Sci.*, 2021, **8**, 2103314.
19. Q. Z. Qian, Y. P. Li, Y. Liu, L. Yu and G. Q. Zhang, *Adv. Mater.*, 2019, **31**, 1901139.